Deciphering Branched Galactomannan Structures via Multistage Ion Mobility MS and MS n Fragmentation (Multistage IMS n)

Rania Benazza, Mathieu Fanuel, Hélène Rogniaux, David Ropartz

Rapid Communications in Mass Spectrometry

WILEY

Rapid Communications in Mass Spectrometry

RESEARCH ARTICLE OPEN ACCESS

Deciphering Branched Galactomannan Structures via Multistage Ion Mobility MS and MS^n Fragmentation (Multistage IMS^n)

Rania Benazza[1,2] | Mathieu Fanuel[1,2] | Hélène Rogniaux[1,2] | David Ropartz[1,2]

[1]INRAE, UR BIA, Nantes, France | [2]INRAE, PROBE Research Infrastructure, BIBS Facility, Nantes, France

Correspondence: David Ropartz (david.ropartz@inrae.fr)

Received: 22 April 2025 | **Revised:** 13 June 2025 | **Accepted:** 16 June 2025

Funding: This work was supported by Agence Nationale de la Recherche, AMETHYST project of the PEPR DIADEM, France 2030 program (project number ANR-22-PEXD-00).

Keywords: galactomannan | hemicellulose | IMS | multistage IMS^n | oligosaccharides

ABSTRACT

Rationale: Hemicelluloses are abundant carbohydrate components in plant cell walls. They play a crucial structural role in binding cellulose microfibrils, in addition to other biological functions. Their high structural variability directly influences their biological properties, making it important to establish a structure–function relationship. In the case of galactomannans, this complexity lies in branching, large size, in addition to isomerism, which makes their characterization challenging. In this context, we have demonstrated that cyclic ion mobility spectrometry (IMS), combined with porous graphitic carbon (PGC) chromatography, mass spectrometry (MS), and multistage MS/MS fragmentation (IMS^n), is a powerful tool for the detailed elucidation of galactomannan structures.

Methods: In this study, we show that our multistage IMS^n sequencing approach, previously validated for homo-linear oligosaccharides (OS), can be successfully applied to hetero-branched hemicelluloses with careful adjustments. Our approach consists of building a database (DB) library of high-resolution IMS (HR-IMS) profiles of disaccharidic and trisaccharidic fragments. Then, the sequence of the oligosaccharide of interest is retrieved by comparing the HR-IMS profile of its disaccharidic and trisaccharide fragments with the profiles from the DB library.

Results: In fact, our IMS^n experiments on galactomannan reveal arrival time distribution (ATD) profiles matching with known reference structures, confirming the co-existence of multiple isomers. In addition, we proved that this approach could be improved by incorporating trisaccharidic fragments to our DB library, serving in the characterization of higher degree of polymerization (DP) structures (DP4 in this case).

Conclusions: Overall, this work paves the way for the characterization of even more complex oligosaccharides, which can be potentially used for bio-based material conception.

1 | Introduction

Cell wall polysaccharides are classically divided into cellulose, hemicellulose, and pectin, which represent the majority of the plant cell wall, along with proteins and, in the case of secondary cell walls, phenolic compounds [1]. Hemicelluloses are β(1–4)-linked sugars in equatorial configuration, forming structurally distinct classes such as xyloglucans, xylans, mannans, glucomannans, and mixed β(1–4), (1–3)-glucans. Although they are abundant in many plant species, they show very distinct

structural details in different species and different plant cell types [1].

The major role of hemicelluloses is to strengthen the cell wall by tethering cellulose microfibrils [2], but they are also responsible for—or involved in—many other biological functions in primary and secondary cell walls, like cell expansion [2, 3], seed storage, and molecules signalling [1].

Beyond their structural and biological roles in plant cell wall, plant-based polysaccharides are increasingly recognized for their potential as promising eco-friendly and sustainable biomaterials. Due to their abundance, biocompatibility, and biodegradability, they are replacing synthetic materials in biomedical engineering, food packaging, and agricultural or industrial purpose for greener chemistry [4].

The functions and properties of polysaccharides for the aforementioned industrial applications are highly related to their structures; although these structures vary considerably at different levels. The variability can occur in the number of constituent subunits, the nature of these subunits, and the nature of their linkage. In addition to their isomeric heterogeneity, the presence of chemical modifications and branched chains on polysaccharides adds a supplementary level of complexity to their structure. It is therefore necessary to finely characterize these polysaccharides in order to better understand the impact of all these structural details on their function, so as to be able to control them closely and adjust their properties to targeted uses.

Common analytical tools used currently for the characterization of oligosaccharides (OS) lack speed and sensitivity. Nuclear magnetic resonance spectroscopy (NMR), although highly informative, requires a large amount of material, in addition to extensive analysis time [5]. Mass spectrometry (MS)-based approaches provide valuable information on the direct measurement of OS, however cannot fully resolve their structures due to the isomers' inherent complexity [6]. MS can be coupled to liquid chromatography (LC), such as hydrophilic interaction LC (HILIC-MS) [7–9] and porous graphitic carbon (PGC-MS) [10–12] for neutral OS, to separate isomers prior to their MS analysis. However, due to the limitation of classical MS/MS approach (collision induced dissociation, CID) to produce informative fragments, the method often fails to enable the structural characterization of the separated isomers. On the other hand, IMS is a robust and reproducible method that has the ability to tackle the isomerism challenges, if the modifications impact the conformation of the ion in gas phase. IMS is based on measuring the mobility of ions in a buffer gas and under the effect of an electric field and thus depends on the ions' conformation under these conditions [13]. Current state-of-the-art IMS instruments, achieve high resolutions, making it possible to decipher the challenges encountered in separating isomeric molecules. Structures for Lossless Ion Manipulation (SLIM)-based Travelling Wave Ion Mobility Spectrometry (TWIMS) developed by the group of R. D. Smith [14] can theoretically reach a resolving power (Rp) of 600 when travelling the 13-m drift tube 100 times. Giles et al. [15] also presented Cyclic IMS as the highest resolution commercially available IMS device, using the TWIMS method as well. It has been proved that an Rp up to 900 for OS characterization can be reached upon increasing the number of passes in the 1-m cyclic racetrack [16]. In addition to access to very high-resolution ion mobility, the clear advantage of this instrument is that it can combine ion mobility and MS/MS on several stages, making the cyclic IMS a powerful tool in glycosciences.

Although not applied in this study, collision cross section (CCS) measurements can be derived from mobility measurements obtained from cyclic IMS analysis. Xia et al. introduced a calibration strategy designed specifically for multipass cyclic IMS, enabling accurate CCS determination of four isomeric trisaccharides [17].

IMS has emerged as a powerful technique for glycosciences, capable of separating specific types of glycan isomers as shown in several key studies. For instance, Manz et al. showed that IMS could effectively characterize isomeric structures from released N-glycans [18]. Earlier studies also highlighted the utility of IMS in glycan analysis [19–22].

More recently, the group of T. R. Rizzo has made significant contributions in the area of glycan analysis, especially focusing on the combination of SLIM and cryogenic infrared (IR) spectroscopy to separate and identify glycans, enabling detailed structural elucidation of glycan mixtures [23–26].

Our group used cyclic IMS to sequence linear homo-oligosaccharides using a multistage IMS^n approach. The first step is to build up a database of HR-IMS profiles of monosaccharides and disaccharides. Then, the sequence of the oligosaccharide of interest is retrieved by comparing the HR-IMS profile of its monosaccharide fragments (to define the sequence in terms of building blocks) or disaccharide fragments (to define the sequence in terms of the branching pattern, including anomerism and positional isomerism) with the profiles stored in the databank. The benefits of this approach allowed mainly to tackle the isomerism challenges within carbohydrates, which helped understand the gas-phase behavior of galactofuranosides in a study by Ollivier et al. [27] and was expanded to the structural elucidation of enzymatically produced mannosides [28]. Additionally, Van de Put et al. used a similar strategy, based on cyclic IMS separation and pre-store CID fragmentation, to determine the monosaccharide composition and the anomeric configuration of disaccharide isomers within prebiotic galactooligosaccharides [29]. These studies highlight the many advantages of cyclic IMS in overcoming the difficulties of the challenging characterization of OS.

However, hemicelluloses in nature are much more heterogeneous than synthetic OS. For instance, xyloglucans, which represent the majority of the hemicelluloses of the plants primary cell walls, have a high structural complexity due to their branched carbohydrate chains. They are in fact composed of a glucosyl backbone with xylosyl side chains, which can be substituted by a galactose that can potentially be acetylated and/or substituted by a fucose. β(1–4)-linked mannans are also challenging as they can be found as a linear backbone consisting of mannose units, called mannans. They can be substituted by galactose, referred to as galactomannans. They can consist as well of nonrepeating mannose and glucose units, known as glucomannans. They can also be acetylated as in the case of mannans and glucomannans [1]. Each of these structural variations, in addition to isomerism,

can influence the physical and biological properties of OS and push us in advancing analytical tools to characterize these complex structures and better answer these questions.

In this study, we focus on galactomannan structures, which are quite complex due to the presence of galactose ramifications. Accordingly, the aim of this study is to (i) characterize the ramified structures and demonstrate the applicability of our multistage IMS^n approach and (ii) to assess its ability to handle more complex and larger OS structures.

2 | Material and Methods

2.1 | Samples

Branched galactomannan OS including Galα(1–6)-Man(β1–4)Man (code MAN213, hereafter referred to as GM) and the mixture of β(1–4)-linked D-mannopyranosyl units substituted by an α(1–6) D-galactopyranosyl (code MAN215) were purchased from Elicityl (Crolles, France). Branched Man(β1–4)Man-Galα(1–6) (code GMM3, hereafter referred to as MG) as well as linear mannotriose (Man (β1–4)Man (β1–4)Man, code O-MTR, hereafter referred to as M3) were obtained from Megazyme (Wicklow, Ireland). The structure of the samples following Haworth projection is represented in Figure 1.

2.2 | Chemicals

HPLC grade methanol (MeOH), acetonitrile (ACN) and water (H_2O) were purchased from Carlo-Erba (Val de Reuil, France). Lithium chloride (LiCl) was obtained from Sigma-Aldrich (Saint Quentin Fallavier, France).

2.3 | IMS-MS Experiments

IMS-MS analyses were performed on a SELECT SERIES Cyclic IMS (cIMS) instrument (Waters, Wilmslow, UK). OS were infused at a concentration of 0.5–25 μg/mL in 50:50 H_2O/MeOH depending on the purity of the sample, through a syringe pump set at a flow rate of 5 μL/min. Lithium adducts were generated upon samples doping with 0.1-mM LiCl. The Z-spray ESI source parameters were set as follows: the capillary voltage at 2.8 kV, the cone voltage at 80 V, the source temperature at 100°C, the desolvation temperature at 300°C, and the nebulizer pressure at 6 bar. Of note, the capillary voltage and cone voltage were both increased to 3 kV and 160 V, respectively, to boost higher

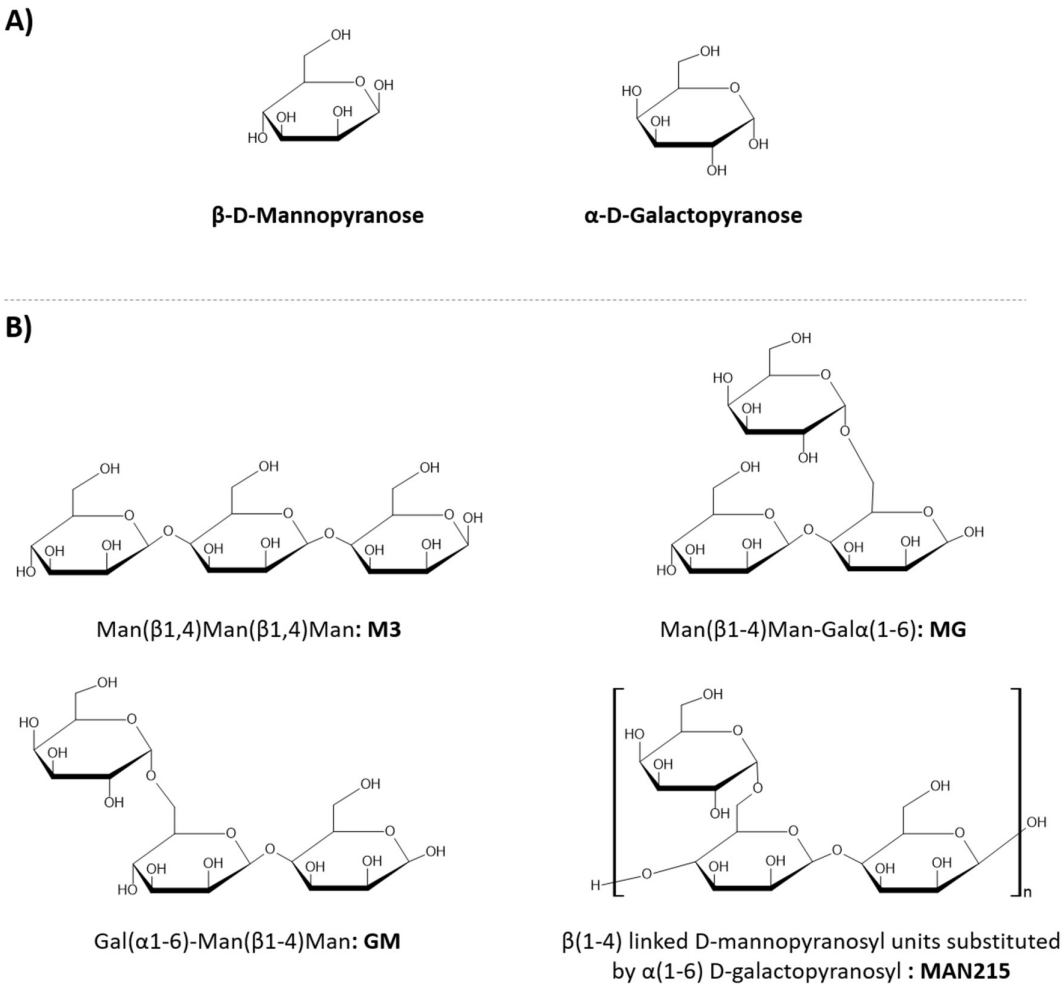

FIGURE 1 | (A) Representation of the studied monosaccharides and (B) the standard DP3 oligosaccharides (M3, MG, and GM) along with the MAN215 sample following Haworth projection.

DP structures ionization. IMS separations were performed in static mode with a cyclic and array traveling wave (TW) velocity both at 350 m/s and a TW static height of 16 V. The IMS-MS parameters are detailed in Text S1. Top and tail (TT) experiments were carried out in the IMS to clean the samples and obtain distinct IMS profiles for each structure (Figure S1). OS sequencing was performed as well in the pre-store where an optimized CID collisional energy for each sample was applied on the slices of interest to release the fragments of interest (Table S1). To ensure the validity of our analyses, we consistently monitored GM standard sample prior to each experiment and determined the IMS features and drift time (t_D, in ms) after 4 and 8 passes. The observed variation in tD values for both 4 and 8 passes remained within ±0.13 ms, which we consider acceptable for subsequent analyses (Figure S2).

2.3.1 | LC-IMS-MS Experiments

Acquisitions were performed with the same IMS and MS parameters than for classical IMS-MS experiments previously detailed. Here, the mass spectrometer was coupled with an Acquity H-Class UHPLC system (Waters, Manchester, UK) equipped with a Hypercarb Porous PGC column (100 × 1 mm, particle size 3 µm from Thermo-Fischer Scientific, Courtaboeuf, France) heated at 80°C. Elution was performed at a flow rate of 0.165 mL/min. The gradient was optimized in order to separate the different conformers of DP3 and DP4 species (Figure S3) and was as follows: 0–33 min at 0%–20% B; 33–34 min at 20%–80% B; 34–38 min at 80% B; 38–45 min at 80%–0% B where A is water and B is acetonetrile. In LC-IMS-MS/MS experiments, the energy in the trap cell was optimized depending on the nature of the fragments of interest (Table S2).

2.3.2 | Data Analysis

All obtained spectra were recorded using the Quartz software on the cIMS instrument (Waters Embedded Analyser release 9, Waters, Wilmslow, UK). Data processing was performed on Masslynx v4.2 and Driftscope v2.9 (both from Waters, Wilmslow, UK). Arrival times (t_A) were corrected to give drift times (t_D) to compare the effective separation time of the fragments with the reference standards. This was done by simply subtracting the duration of all events prior to the separation time. ATDs smoothing was performed using the Stravizky–Golay algorithm (window size = 1, number of smooths = 2). Gaussian fitting of the extracted ATDs was done on CIUSuite2 software with the following parameters: minimum peak amplitude = 0.01, maximum components = 6, expected peak width = 2, and peak width tolerance = 1.

3 | Results and Discussion

3.1 | Enrichment of the Database Library: Addition of New Fingerprints

In order to produce an efficient IMS database library for fragments, we chose to dope our samples with LiCl and we focused on $[M + Li]^+$ ions in all experiments, because it is reported that Li adducts yield higher intensity fragments upon CID experiments of OS, compared to Na adducts for instance [27].

The three trisaccharides representative of the different branching patterns found in galactomannans are commercially available as follows: Man(β1,4)Man(β1,4)Man: M3, Gal(α1–6)-Man(β1–4)Man with the galactose branched on the nonreducing end: GM, and Man(β1–4)Man-Galα (1–6) with the galactose branched on the reducing end: MG (Figure 1). We used these trisaccharides (i) to register disaccharides' and monosaccharides' fragments IMS fingerprints to complete our database and (ii) to validate the fact that the fingerprints measured are independent from the lateral branching of the galactose in (α1,6) in the different positions.

In a first step, each trisaccharide was analyzed independently. We selected the cIMS parameters (Text S1) that were able to differentiate between the trisaccharidic standards (three isomers), where the number of separations was set to 8 passes (Figure S4A). The three standards (M3, MG, and GM) exhibited each a distinct distribution after 8 passes, upon selection of a mass corresponding to DP3 species ($[M + Li]^+$, *m/z* 511.2). However, we show that each species exhibits multiple IMS peaks. Considering that, each species can have several conformations, we cannot conclude whether the conformations come from a single species or whether there is a contamination by the presence of several isomers (as exemplified for M3 that presents two IMS peaks at 124.20 and 126.44 ms, and for GM that presents a peak shoulder before the major IMS peak at 132.48 ms). To validate the specific fingerprints, we therefore carried out PGC-IMS-MS analysis on the DP3 species (Figure S5). The aim of these experiments is (i) to determine the number of real isomers with the chromatographic scale and (ii) to obtain the structural information through IMS/MS.

Indeed, when using PGC-IMS-MS (Figure 2), the M3 presents a bimodal distribution with two specific features at 124.11 and 126.35 ms (corrected t_D), thus, two conformations instead of only one that was observed in IMS-MS experiments (Figure S4). GM also presents a bimodal distribution with baseline resolved peaks at 127.14 and 132.42 ms. Here, we notice the disappearance of the peak shoulder observed in direct infusion preceding the major peak, with the appearance of the supplementary conformation observed when using PGC, at 127.14 ms. This conformation has a t_D close to that from M3 (~126.44 ms in M3, Figure S4), and thus was lost at the prepurification step via top and tail experiments. For MG, a single peak at 130.44 ms was observed (Figure 2A), in-line with the results from IMS-MS.

Overall, the observed features for M3 and MG using PGC-IMS-MS were comparable with those observed through direct infusion. However, in the case of GM, when using PGC-IMS-MS, we noticed the presence of a distinct feature at 127.14 ms that was not observed in direct infusion. This feature could have been lost during slicing experiments (Figure S1), where the sample containing the GM isomer was present in the mixture with other structures that overlapped with its second feature. This step highlighted the complementarity of PGC and ion mobility when it comes to building a database library of IMS profiles. Thus, we chose to keep the ATD profiles obtained through PGC-IMS-MS for the DP3 species.

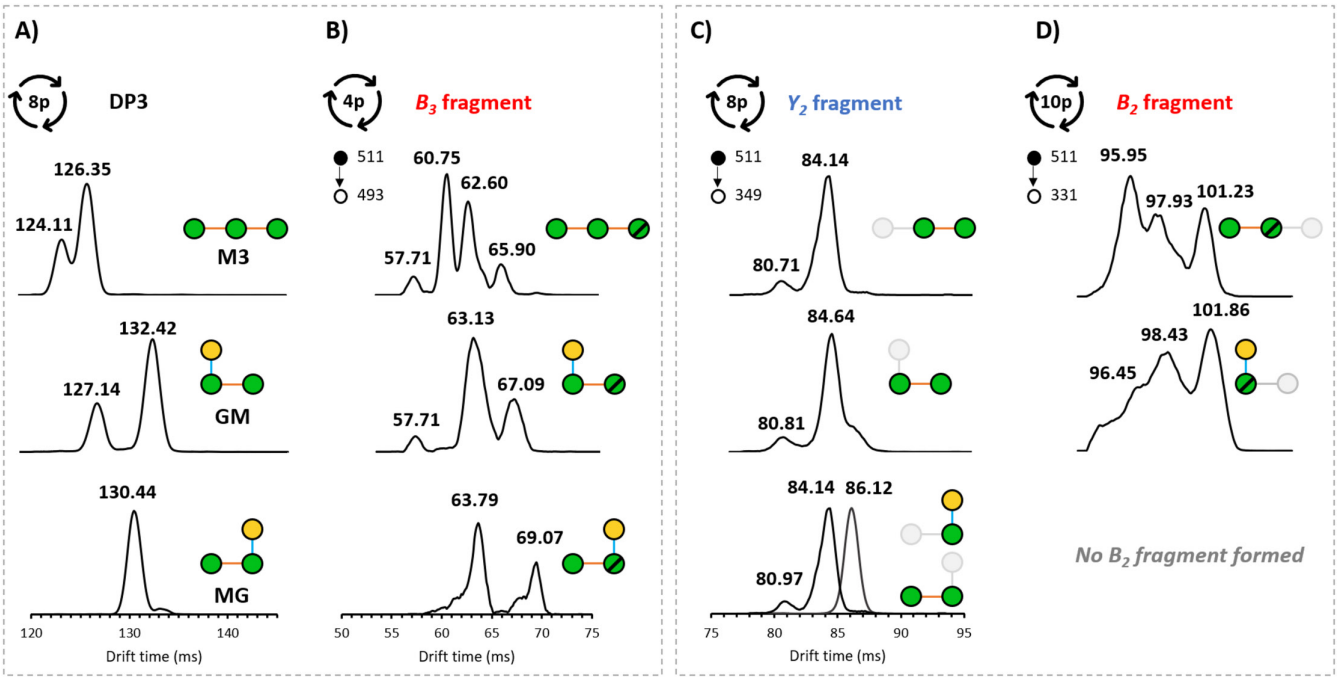

FIGURE 2 | PGC-IMS signature profiles of standard trisaccharides (DP3: $[M+Li]^+$, 511.2 m/z) and their CID fragments. (A) IMS profiles of M3 (top), GM (middle), and MG (bottom) after 8 passes in the cyclic IMS. (B) The obtained B_3 ($[M+Li]^+$, m/z 493.2) fragments upon dehydration of DP3 species. (C, D) The obtained disaccharidic fragments, at the reducing end (Y_2: $[M+Li]^+$, 349.1 m/z) and at the nonreducing end (B_2: $[M+Li]^+$, 331.1 m/z). Galactose units are depicted in green circles, while mannose units are depicted in yellow. Dashed circles indicate the presence of a double bond.

Each standard was then fragmented, and the signature of the product ions (i.e., *Y* and *B* product ions) was registered. A CID energy of 100–120 eV was applied to the three species in the pre-store of the IMS cell, followed by the IMS measurement of the resulting fragments, following a strategy previously described by our group [27]. In theory, the fragmentation of oligosaccharide ions under CID conditions leads to the production of fragments that contain the reducing (*Y*- and *Z*-type ions) and the nonreducing (*B*- and *C*-type ions) ends [30]. This can be a problem because these fragments can be isobaric due to the symmetry of the molecule (m/z of fragment $Y = m/z$ of fragment C and m/z of fragment $Z = m/z$ of fragment B). However, in the cyclic IMS, previous studies [27] showed that, when working with nitrogen as a collision gas in the transfer, trap, or pre-store cell, the *C* and *Z* fragment ions are minor (100-fold lower [if any] than *Y*- and *B*-type ions), which leads us to focus only on the latter fragments to determine the IMS profiles (Figure S6). A specific sequence of separation was applied for each fragment.

In a first step, we attempted to produce *B3* fragments by applying a pre-store energy on DP3 species. However, since *B3* fragments are a dehydrated form of intact *Y3* ions, they appear with very low intensity, which makes their detection difficult after ion mobility separation (data not shown). To address this limitation, *B3* fragments were obtained via fragmentation of pure DP3 structures in the trap cell, where the energy was finely tuned by increasing slightly the cone voltage in order to induce pseudo-B_3 formation (Figure 2B).

The three species exhibited each distinct *B3* fragment ($[M+Li]^+$ at m/z 493.2) profiles after 4 passes in the cyclic IMS. M3 presents a multimodal distribution with peaks at 57.71, 60.75, 62.60, and 65.90 ms. GM presents, as well, a multimodal distribution with features at 57.71, 63.13, and 67.09 ms. For MG, the profile presents a bimodal distribution with peaks at 63.79 and 69.07 ms, with a minor contribution of other conformations, which allows distinguishing this fragment from the prior characterized ones. In general, the pseudo-fragmentation of DP3 species produced distinct profiles enabling the differentiation between the three isomers.

Next, the product ions, which correspond to the disaccharides, are analyzed (i.e., specificity of the branching pattern in our sequencing strategy), and their signatures are presented in Figure 2C,D. Y_2 fragment at m/z 349.1 and B_2 fragment at m/z 331.1 were, respectively, submitted to 8 and 10 passes in the cyclic cell.

The Y_2 fragment ($[M+Li]^+$ at m/z 349.1) produced from the fragmentation of the M3 showed a bimodal distribution (peaks at $t_D = 80.71$ and 84.14 ms). The B_2 fragment was also detected ($[M+Li]^+$ at m/z 331.1) and showed a multimodal distribution with peaks at 95.95, 97.93, and 101.23 ms (corrected t_D), corresponding to the mannobiose structure at the nonreducing end. The observed matches of the Y_2 and B_2 fragments with the IMS profiles of the mannobiose structures stored in the database confirm (i) the structure of the starting M3 and (ii) the validity of the sequencing approach.

For GM, the same IMS signature was observed for the Y_2 fragment ($[M+Li]^+$ at m/z 349.1), confirming its mannobiose unit at the reducing end. However, a new B_2 fragment signature was detected with peaks at 96.45, 98.43, and 101.86 ms (corrected t_D),

which gives a new specific signature of the (α1,6)Gal-Man unit at the nonreducing end that allows us to add a new fingerprint to our DB library.

From the analysis of the MG, no B_2 ions signal was obtained. However, a complex Y_2 fragment profile that corresponds to the measurement of the $[M+Li]^+$ at *m/z* 349.1 was observed. To clarify this point, slicing experiments on the different Y_2 IMS peaks were performed. This revealed two distinct signatures; the first corresponding to the fingerprint of the mannobiose with peaks at 80.97 and 84.14 ms (corrected t_D), the second is a new signature with a single IMS peak at 86.12 ms. From the structure of the MG, the fragment that corresponds to the mannobiose is a *Yα* resulting from the loss of the reducing end galactose. From that, the new signature obtained is the real fingerprint of the (α1,6)Gal-Man.

Remarkably, this sample exemplifies the challenges that can be encountered upon the fragmentation of ramified OS. Whereas multiple Y_n fragments were generated and confirmed the ramified structure, the lack of B_2 fragments that should reinforce our interpretation shows that branching information could be lost due to the consecutive fragmentation pathways.

Overall, the features observed at both trisaccharide extremities show distinct fingerprints that allow confirming their structure and can serve as new reference fingerprints. Even if signatures seem to be complex (as shown for the B_2 fragments from M3 and GM), their deconvolution upon Gaussian fitting of their t_D profiles (Figure S7) exhibits distinct multimodal distributions that allow their differentiation with sufficient clarity.

In a final step, the product ions, which correspond to the monosaccharides, are analyzed, as shown in Figure S8. Y_1 fragment at *m/z* 187.1 and B_1 fragment at *m/z* 169.1 were, respectively, submitted to 6 passes (including 4 static and 2 ramped waves) and 2 passes in the cyclic cell.

M3 fragmentation produced mannose Y_1 ($[M+Li]^+$, *m/z* 187.1) and B_1 ($[M+Li]^+$, *m/z* 169.1) fragments, as expected. The Y_1 fragment exhibited a single peak at $t_D = 39.33$ ms, while B_1 showed a bimodal distribution with a major peak at 14.25 ms and a minor one at 15.70 ms (corrected t_D). As expected, the IMS profiles correlated perfectly with mannose units at both extremities as stored in the library (Figure S8). Surprisingly, for GM and MG, the same fragmentation patterns were observed as in the case of M3, which would indicate the presence of mannose units at both extremities. From these results, the branched galactose units are mainly not observed upon CID fragmentation. Our hypothesis is that the lack of information on the galactose branching is due to the lithium adduct being preferentially coordinated on the mannose main chain. The fragmentation would then mainly produce a "neutral loss" of galactose and thus would prevent the complete assignment of monosaccharidic fragments. However, it is worth noting that the B_1 fragment stemming from the dissociation of each reference presents a slightly different profile. This difference is reflected in the relative intensity of the second feature measured at 15.70 ms for the M3, 15.93 ms for the GM, and 15.82 ms for the MG. Indeed, this feature is signature of the mannose B_1 fragment, which can be different according to the position of the double-bond formed based on the particular nature of the glycosidic-bond cleaved [31].

To conclude this part, these results led to a modification in our strategy because of the lack of information provided by monosaccharides for hetero-branched OS. However, the use of disaccharide fragments does not appear to be sufficient due to the possibility of a neutral loss of the laterally branched galactose (as exemplified for the MG structure). We showed that the

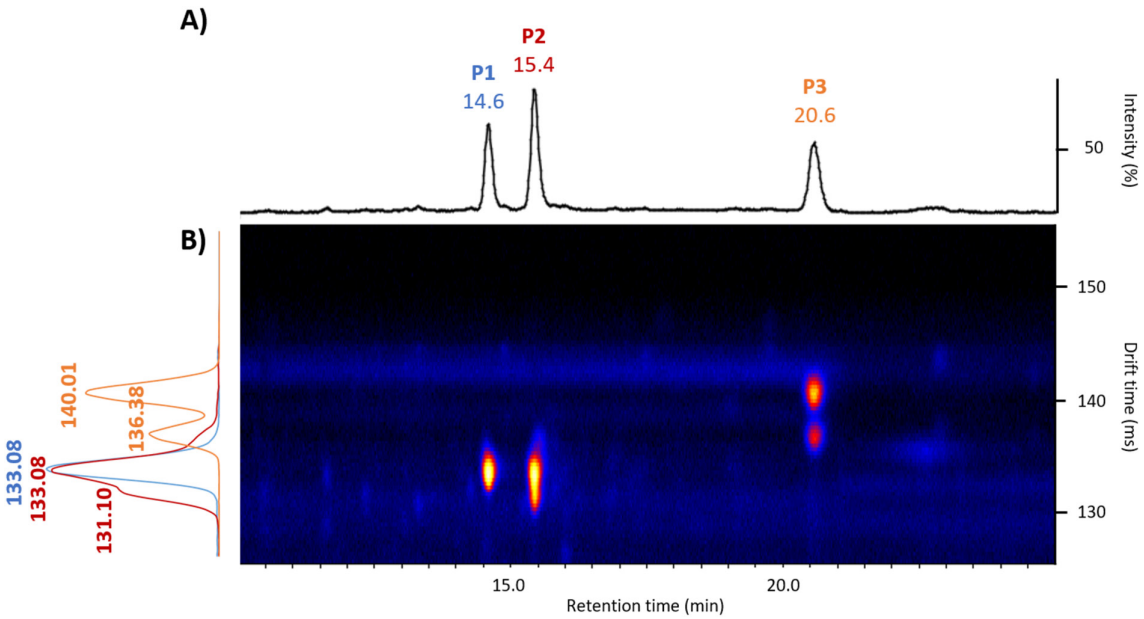

FIGURE 3 | PG-IM-MS experiments of MAN215 DP4 species ($[M+Li]^+$, m/z 673.2). (A) Extracted chromatogram obtained using the PGC column at 80°C, revealing three baseline-resolved isomers at 14.6, 15.4, and 20.6 min. (B) Heatmap of the separated isomers revealing the different features of each isomer, with a single distribution for the first isomer (blue) at 133.08 ms, a major feature for the second structure (red) at 133.08 ms with a peak shoulder at 131.10 ms, and a bimodal distribution for the last isomer (orange) with features at 136.38 and 140.01 ms.

trisaccharide standards exhibit unique IMS fingerprints, allowing for confident structural discrimination; thus, we decided to complete the database signature with the profiles of Y_3 (the profiles of the trisaccharides) and B_3 for the study of larger species.

3.2 | Insights From Multistage IMS^n Experiments

To validate our approach, glycan structures that consist of enzymatic digestion of a galactomannan oligosaccharide were studied by IMS^n experiments. MAN215 (from Elicityl) contains multiple DP species (from DP2 to DP9) with potential isomers for each DP depending of the branching of galactopyranosyl units (Figure 1).

The DP4 of the MAN215 was studied by IMS-MS in direct infusion. We selected in the quadrupole a mass corresponding to DP4 species ($[M+Li]^+$, *m/z* 673.2) after injecting the sample in similar MS conditions than the previously analyzed DP3 species. Figure S9A shows the mobilogram obtained after 6 passes in the cyclic IMS. In the first place, we performed slicing experiments to separate the different conformers, which were subjected to 6 passes in the mobility cell. This resulted in four distinct IMS peaks depicted in Figure S9B–E with C1, C2, C3, and C4 at 132.02, 133.77, 136.64, and 140.87 ms, respectively.

As demonstrated for the M3 (Figures 2 and S5), a single structure can adopt different conformations thus providing different peak in IMS. To correlate the number of conformations detected and the real number of structures in the sample, the PGC-IMS-MS approach was used for DP4 species analysis (Figure 3).

Indeed, at the chromatographic scale, the separation reveals three baseline-resolved peaks, hence three different isomers. The first isomer is observed at 14.6 min and presented one conformation measured at 133.08 ms (P1) by IMS. The second isomer eluting at 15.4 min presented two different conformations with IMS peaks at 131.10 and 133.08 ms (P2). Finally, the last isomer eluted at 20.6 min and presented a bimodal IMS peak distribution at 136.38 and 140.01 ms (P3) (Figure 3A).

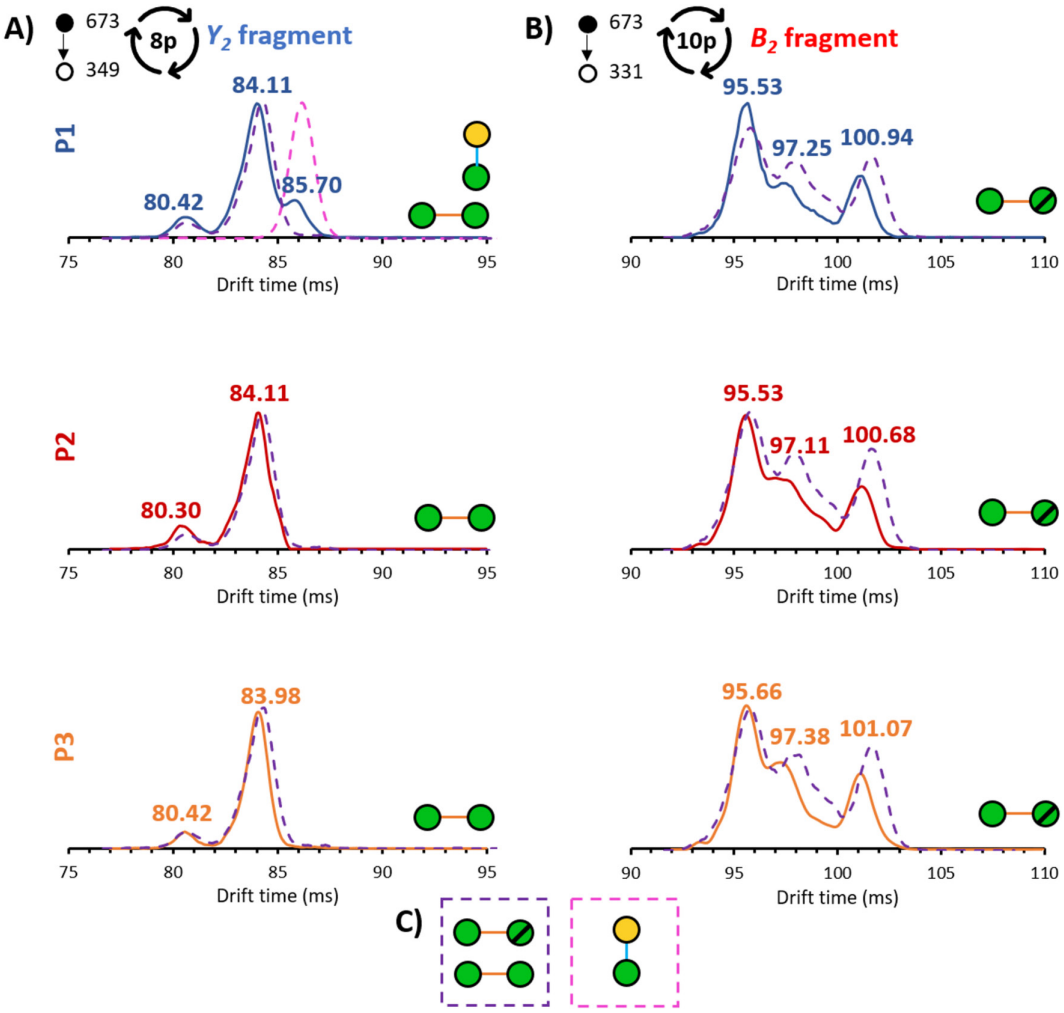

FIGURE 4 | PGC-IMS profiles of disaccharidic fragments (A) Y_2: $[M+Li]^+$, m/z 349.1 after 8 passes and (B) B_2: $[M+Li]^+$, m/z 331.1 after 10 passes, obtained upon the fragmentation of the three MAN215 DP4 species separated through PGC-IM-MS (P1, P2, and P3; $[M+Li]^+$, m/z 673.2). The ATD profiles of the reference standards are represented in dashed lines with (C) their SNFG representation. Galactose units are depicted in green circles, while mannose units are depicted in yellow. Dashed circles indicate the presence of a double bond.

These observations highlight the complementarity of PGC and IMS to address the problem of the structural study of complex mixtures of OS. Indeed, the conformations C1 and C2 observed in IMS-MS experiments (Figure S9B,C) correspond to the P1 isomer observed in PGC, confirming the presence of a first distinct DP4 structure. However, the C2 feature observed at 133.77 ms in IMS-MS (Figure S9C) could also match with the one corresponding to the P2 isomer in PGC that elutes at 15.4 min. This poses a real challenge, since both isomers (P1 and P2 in Figure 3) share a common feature at 133.08 min. In contrast, the conformations C3 and C4 obtained through direct infusion (Figure S9D,E) correspond clearly to the isomer eluting at 20.6 min (P3), highlighting the complementarity of both approaches.

From these experiments, we obtain the specific IMS signatures of each DP4 isomers with the contribution of all conformations, allowing the production of comprehensive product ion profiles.

3.3 | Can We Go Further and Sequence Higher DP Species?

We then applied our sequencing strategy on each DP4 efficiently separated by PGC. Figure 4 shows the mobilograms obtained from the sequencing of MAN215 DP4 species ($[M+Li]^+$, *m/z* 673.2) compared to reference fragments. At the reducing extremity, there are mainly peaks corresponding to mannobiose observed for P1, P2, and for P3. P1 exhibits an additional peak corresponding to the galactosyl-mannose unit. On the nonreducing end, B_2 fragments matched mainly with mannobiose disaccharide for all isomers, i.e., P1, P2, and P3. In these experiments, disaccharidic fragments showed very similar features, with slight differences regarding the Y_2 fragment for the first conformer (P1) at 85.70 ms. Therefore, the high similarity in the profiles of the B_2 and Y_2 fragments does not allow a definitive assignment of the tetrasaccharidic structures of P1, P2, and P3.

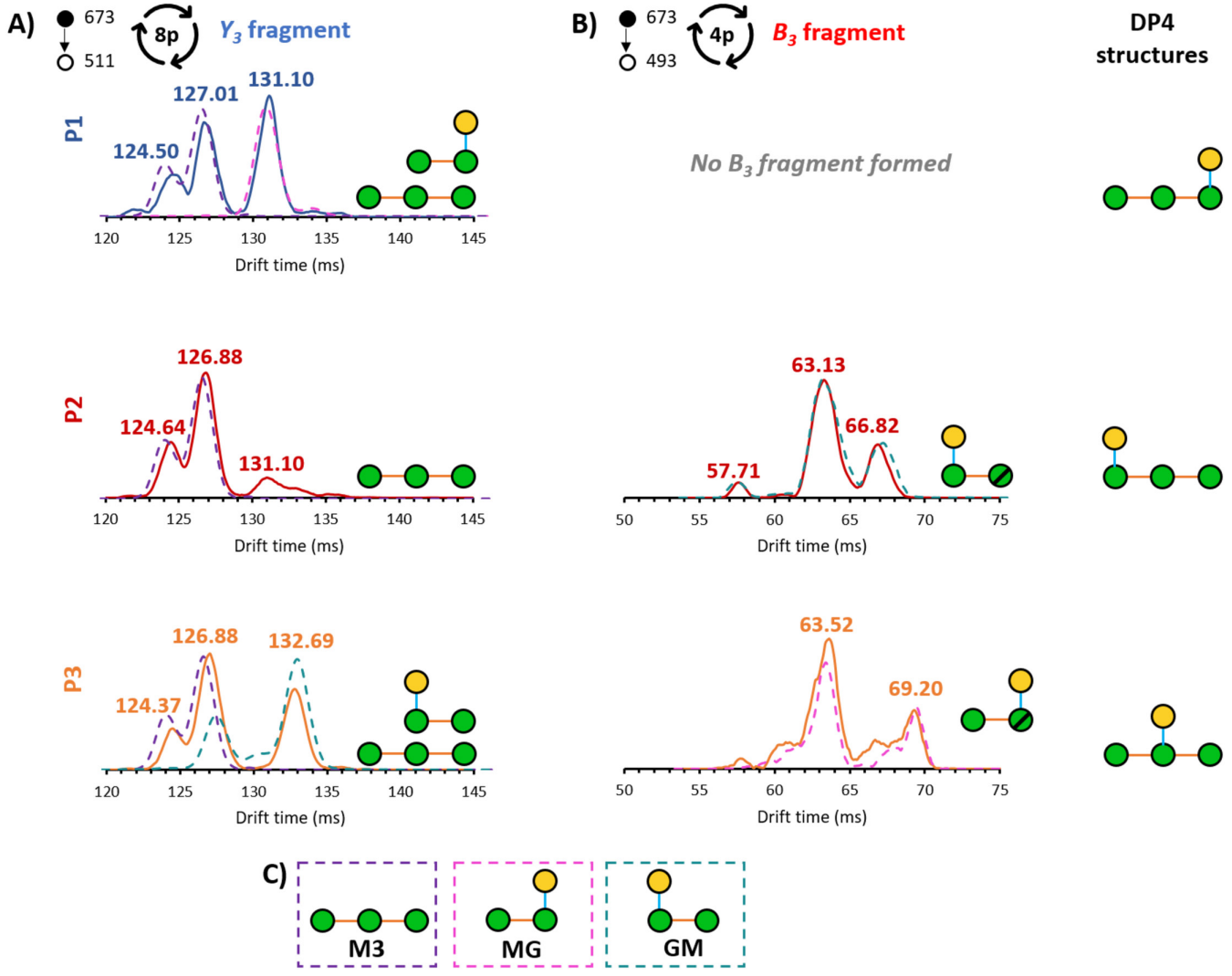

FIGURE 5 | PGC-IMS profiles of trisaccharidic fragments (A) Y_3: $[M+Li]^+$, m/z 511.2 after 8 passes and (B) B_3: $[M+Li]^+$, m/z 493.2 after 4 passes, obtained upon the fragmentation of the three MAN215 DP4 species separated through PGC-IM-MS (P1, P2, and P3; $[M+Li]^+$, m/z 673.2). The characterized DP4 structures of P1, P2, and P3 are depicted in SNFG representation. (C) SNFG representation of trisaccharide references with their corresponding color. Galactose units are depicted in green circles, while mannose units are depicted in yellow. Dashed circles indicate the presence of a double bond.

Once again, as discussed for the trisaccharides sequencing, the disaccharide product ions are not sufficient. We considered trisaccharidic fragment profiles previously registered for the characterization of DP4 structures. Alignments are shown in Figure 5. The IMS profile obtained for the Y_3 of P1 revealed the contribution of two species. First, a doublet at 124.5 and 127.01 ms that can be attributed to the Y_3 of M3, and a single peak at 131.10 ms that is attributed to the Y_3 of MG. From that, P1 was identified as a linear M3 backbone with a galactose branched at the reducing extremity. The absence of the B_3 product ion supports this attribution, as explained for the results presented in Figure 2 (absence of B_2 on the MG standard that has the galactose branched on the reducing end mannose).

For P2, the IMS profile obtained for the Y_3 corresponds to the signature of M3 (doublet at 124.64 and 126.88 ms). Of note, a minor peak detected at 131.10 ms was unexpectedly observed at the reducing end. This signal may originate from the preceding P1 structure, as slight carryover given the heterogeneity of the sample. The IMS profile of the B_3 matches the pseudo B_3 GM standard distribution (57.71, 63.13, and 66.82 ms). All these results show that P2 is a linear M3 backbone with a galactose branched at the nonreducing extremity.

Finally, the Y_3 signature of the P3 exhibited two co-existent conformations at the reducing extremity corresponding to M3 (124.37 and 126.88 ms) and GM (126.88 and 132.69 ms), with a B_3 fragment signature that corresponds to the one from MG (63.52 and 69.20 ms). All these measurements show that P3 is a linear M3 backbone with galactose branching at the central mannose.

To conclude, our sequencing strategy enabled the characterization of branched DP4 structures. The optimized LC gradient, combined with high-resolution IMS measurements, provided clear information on the number of isomers present in a complex biological sample, with distinct IMS profiles. While disaccharidic fragments offered limited structural differentiation for DP4 species, the trisaccharidic fragments provided highly informative insights, revealing the identity of each isomer. In summary, we could prove via our sequencing strategy the variability in DP4 structures in the MAN215 sample, which correspond here to linear mannobiose bearing galactose branching either at the reducing extremity (P1), nonreducing extremity (P2), or at the central position (P3).

4 | Conclusion

Throughout this study, we expanded the applications of cyclic IMS to the determination of HR-IMS profiles of OS derived from branched polysaccharides. This work has highlighted several limitations that make, in our hands, the characterization of ramified OS rather tricky through these IMS^n strategies. One of the main challenges is the potential loss of lateral chain. We approached this difficulty by focusing instead on disaccharidic and trisaccharidic fragments that provide valuable information (contrary to the monosaccharide signatures). The reference fingerprints were then compared with the unknown structures to define their identity. We note that, our study is the first, to our best knowledge, to focus on branched OS characterization, completing our previous contributions on linear OS sequencing using multistage IMS^n.

While our multistage IMS^n strategy offers significant advantages for linear and branched carbohydrates characterization, it is important to acknowledge its limitations. Admittedly, when pure standards are available, the method is more effective. However, when the unknown samples would not match any of our references, their structural characterization can become challenging. In this case, a form of de-novo sequencing could be performed, by building a database from fragments generated within the unknown sample itself.

One of the limitations also that could be encountered is when the fragment ions could not be resolved in the IMS dimension and thus hinder the interpretation. However, we note that the number of IMS passes in the cyclic device is (hypothetically) limitless; therefore, we are optimistic for improving the IMS separation.

Our aim is to extend our refined approach to the characterization of other structurally coplex hemicelluloses, such as xyloglucans and glucomannans, which can also occur in acetylated forms [1]. To strengthen our characterization capability and fulfill this ambition, we could consider, in addition to IMS, higher-energy fragmentation data. Indeed, methods such as electron-based dissociation (electron activated dissociation methods (ExD [32, 33]) or helium-charge transfer dissociation (He-CTD [34, 35])) and photon-based dissociation (extreme UV photon activation (XUVPD [36]) or vacuum ultraviolet (VUV [37])) can pave the way to better understanding oligosaccharide structures and enhance the ability to characterize complex structures.

Author Contributions

Rania BENAZZA: writing – original draft, formal analysis, methodology, data curation, validation, investigation, software. **Mathieu FANUEL:** formal analysis, writing – review and editing, methodology, investigation, data curation, software, validation. **Hélène ROGNIAUX:** writing – review and editing, supervision, project administration, conceptualization, methodology. **David ROPARTZ:** conceptualization, funding acquisition, project administration, writing – review and editing, supervision, methodology.

Acknowledgments

This work is powered by the AMETHYST project of the PEPR DIADEM, with the financial support from the France 2030 program (project number ANR-22-PEXD-0015).

Data Availability Statement

The data that support the findings of this study are available from the corresponding author upon reasonable request.

Peer Review

The peer review history for this article is available at https://www.webofscience.com/api/gateway/wos/peer-review/10.1002/rcm.10100.

References

1. H. V. Scheller and P. Ulvskov, "Hemicelluloses," *Annual Review of Plant Biology* 61, no. 1 (2010): 263–289, https://doi.org/10.1146/annurev-arplant-042809-112315.

2. S. E. C. Whitney, M. J. Gidley, and S. J. McQueen-Mason, "Probing Expansin Action Using Cellulose/Hemicellulose Composites," *Plant*

Journal 22, no. 4 (2000): 327–334, https://doi.org/10.1046/j.1365-313x.2000.00742.x.

3. D. J. Cosgrove, "Expansive Growth of Plant Cell Walls," *Plant Physiology and Biochemistry* 38, no. 1–2 (2000): 109–124, https://doi.org/10.1016/S0981-9428(00)00164-9.

4. Z. Behrooznia and J. Nourmohammadi, "Polysaccharide-Based Materials as an Eco-Friendly Alternative in Biomedical, Environmental, and Food Packaging," *Giant* 19 (2024): 100301, https://doi.org/10.1016/j.giant.2024.100301.

5. H.-Y.-Y. Yao, J.-Q. Wang, J.-Y. Yin, S.-P. Nie, and M.-Y. Xie, "A Review of NMR Analysis in Polysaccharide Structure and Conformation: Progress, Challenge and Perspective," *Food Research International* 143 (2021): 110290, https://doi.org/10.1016/j.foodres.2021.110290.

6. C. J. Gray, L. G. Migas, P. E. Barran, et al., "Advancing Solutions to the Carbohydrate Sequencing Challenge," *Journal of the American Chemical Society* 141, no. 37 (2019): 14463–14479, https://doi.org/10.1021/jacs.9b06406.

7. G. Qing, J. Yan, X. He, X. Li, and X. Liang, "Recent Advances in Hydrophilic Interaction Liquid Interaction Chromatography Materials for Glycopeptide Enrichment and Glycan Separation," *TrAC Trends in Analytical Chemistry* 124 (2020): 115570, https://doi.org/10.1016/j.trac.2019.06.020.

8. G. J. Cavallero and J. Zaia, "Resolving Heparan Sulfate Oligosaccharide Positional Isomers Using Hydrophilic Interaction Liquid Chromatography-Cyclic Ion Mobility Mass Spectrometry," *Analytical Chemistry* 94, no. 5 (2022): 2366–2374, https://doi.org/10.1021/acs.analchem.1c03543.

9. A. G. M. Leijdekkers, M. G. Sanders, H. A. Schols, and H. Gruppen, "Characterizing Plant Cell Wall Derived Oligosaccharides Using Hydrophilic Interaction Chromatography With Mass Spectrometry Detection," *Journal of Chromatography A* 1218, no. 51 (2011): 9227–9235, https://doi.org/10.1016/j.chroma.2011.10.068.

10. Q. Li, Y. Xie, M. Wong, M. Barboza, and C. B. Lebrilla, "Comprehensive Structural Glycomic Characterization of the Glycocalyxes of Cells and Tissues," *Nature Protocols* 15, no. 8 (2020): 2668–2704, https://doi.org/10.1038/s41596-020-0350-4.

11. J. Wei, Y. Tang, Y. Bai, et al., "Toward Automatic and Comprehensive Glycan Characterization by Online PGC-LC-EED MS/MS," *Analytical Chemistry* 92, no. 1 (2020): 782–791, https://doi.org/10.1021/acs.analchem.9b03183.

12. S. Zhou, Y. Huang, X. Dong, et al., "Isomeric Separation of Permethylated Glycans by Porous Graphitic Carbon (PGC)-LC-MS/MS at High Temperatures," *Analytical Chemistry* 89, no. 12 (2017): 6590–6597, https://doi.org/10.1021/acs.analchem.7b00747.

13. V. Gabelica and E. Marklund, "Fundamentals of Ion Mobility Spectrometry," *Current Opinion in Chemical Biology* 42 (2018): 51–59, https://doi.org/10.1016/j.cbpa.2017.10.022.

14. A. V. Tolmachev, I. K. Webb, Y. M. Ibrahim, et al., "Characterization of Ion Dynamics in Structures for Lossless Ion Manipulations," *Analytical Chemistry* 86, no. 18 (2014): 9162–9168, https://doi.org/10.1021/ac502054p.

15. K. Giles, J. Ujma, J. Wildgoose, et al., "A Cyclic Ion Mobility-Mass Spectrometry System," *Analytical Chemistry* 91, no. 13 (2019): 8564–8573, https://doi.org/10.1021/acs.analchem.9b01838.

16. D. Ropartz, A. Lissarrague, M. Jam, et al., "Exploration of the Extracellular Matrix of the Red Alga *Chondrus crispus* Reveals Unprecedented Insights Into Carrageenan Structures," *Carbohydrate Polymers* 348 (2025): 122737, https://doi.org/10.1016/j.carbpol.2024.122737.

17. C. Xia, E. Mernie, J. Zaia, C. E. Costello, and C. Lin, "Accurate Collisional Cross Section Measurement by Multipass Cyclic Ion Mobility Spectrometry," *Analytical Chemistry* 96, no. 29 (2024): 11959–11968, https://doi.org/10.1021/acs.analchem.4c01758.

18. C. Manz, M. Mancera-Arteu, A. Zappe, et al., "Determination of Sialic Acid Isomers From Released *N*-Glycans Using Ion Mobility Spectrometry," *Analytical Chemistry* 94, no. 39 (2022): 13323–13331, https://doi.org/10.1021/acs.analchem.2c00783.

19. Y. Pu, M. E. Ridgeway, R. S. Glaskin, M. A. Park, C. E. Costello, and C. Lin, "Separation and Identification of Isomeric Glycans by Selected Accumulation-Trapped Ion Mobility Spectrometry-Electron Activated Dissociation Tandem Mass Spectrometry," *Analytical Chemistry* 88, no. 7 (2016): 3440–3443, https://doi.org/10.1021/acs.analchem.6b00041.

20. D. J. Harvey, G. E. Seabright, S. Vasiljevic, M. Crispin, and W. B. Struwe, "Isomer Information From Ion Mobility Separation of High-Mannose Glycan Fragments," *Journal of the American Society for Mass Spectrometry* 29, no. 5 (2018): 972–988, https://doi.org/10.1007/s13361-018-1890-5.

21. H. Hinneburg, J. Hofmann, W. B. Struwe, et al., "Distinguishing N-Acetylneuraminic Acid Linkage Isomers on Glycopeptides by Ion Mobility-Mass Spectrometry," *Chemical Communications* 52, no. 23 (2016): 4381–4384, https://doi.org/10.1039/C6CC01114D.

22. J. Hofmann, H. S. Hahm, P. H. Seeberger, and K. Pagel, "Identification of Carbohydrate Anomers Using Ion Mobility–Mass Spectrometry," *Nature* 526, no. 7572 (2015): 241–244, https://doi.org/10.1038/nature15388.

23. P. Bansal, A. Ben Faleh, S. Warnke, and T. R. Rizzo, "Multistage Ion Mobility Spectrometry Combined With Infrared Spectroscopy for Glycan Analysis," *Journal of the American Society for Mass Spectrometry* 34, no. 4 (2023): 695–700, https://doi.org/10.1021/jasms.2c00361.

24. A. Ben Faleh, S. Warnke, P. Bansal, R. P. Pellegrinelli, I. Dyukova, and T. R. Rizzo, "Identification of Mobility-Resolved *N*-Glycan Isomers," *Analytical Chemistry* 94, no. 28 (2022): 10101–10108, https://doi.org/10.1021/acs.analchem.2c01181.

25. S. Warnke, A. Ben Faleh, and T. R. Rizzo, "Toward High-Throughput Cryogenic IR Fingerprinting of Mobility-Separated Glycan Isomers," *ACS Measurement Science Au* 1, no. 3 (2021): 157–164, https://doi.org/10.1021/acsmeasuresciau.1c00018.

26. P. Bansal, V. Yatsyna, A. H. AbiKhodr, et al., "Using SLIM-Based IMS-IMS Together With Cryogenic Infrared Spectroscopy for Glycan Analysis," *Analytical Chemistry* 92, no. 13 (2020): 9079–9085, https://doi.org/10.1021/acs.analchem.0c01265.

27. S. Ollivier, L. Legentil, O. Yeni, et al., "Gas-Phase Behavior of Galactofuranosides Upon Collisional Fragmentation: A Multistage High-Resolution Ion Mobility Study," *Journal of the American Society for Mass Spectrometry* 34, no. 4 (2023): 627–639, https://doi.org/10.1021/jasms.2c00333.

28. S. Ollivier, L. Tarquis, M. Fanuel, et al., "Anomeric Retention of Carbohydrates in Multistage Cyclic Ion Mobility (IMSn): De Novo Structural Elucidation of Enzymatically Produced Mannosides," *Analytical Chemistry* 93, no. 15 (2021): 6254–6261, https://doi.org/10.1021/acs.analchem.1c00673.

29. B. Van De Put, W. J. C. De Bruijn, and H. A. Schols, "Structural Characterization of Disaccharides Using Cyclic Ion Mobility Spectrometry and Monosaccharide Standards," *Journal of the American Society for Mass Spectrometry* 35, no. 5 (2024): 1012–1020, https://doi.org/10.1021/jasms.4c00029.

30. B. Domon and C. E. Costello, "A Systematic Nomenclature for Carbohydrate Fragmentations in FAB-MS/MS Spectra of Glycoconjugates," *Glycoconjugate Journal* 5, no. 4 (1988): 397–409, https://doi.org/10.1007/BF01049915.

31. S. Ollivier, D. Ropartz, M. Fanuel, and H. Rogniaux, "Fingerprinting of Underivatized Monosaccharide Stereoisomers Using High-Resolution Ion Mobility Spectrometry and Its Implications for Carbohydrate Sequencing," *Analytical Chemistry* 95, no. 26 (2023): 10087–10095, https://doi.org/10.1021/acs.analchem.3c01531.

32. J. J. Wolff, T. N. Laremore, H. Aslam, R. J. Linhardt, and I. J. Amster, "Electron-Induced Dissociation of Glycosaminoglycan Tetrasaccharides," *Journal of the American Society for Mass Spectrometry* 19, no. 10 (2008): 1449–1458, https://doi.org/10.1016/j.jasms.2008.06.024.

33. Y. Tang, J. Wei, C. E. Costello, and C. Lin, "Characterization of Isomeric Glycans by Reversed Phase Liquid Chromatography-Electronic Excitation Dissociation Tandem Mass Spectrometry," *Journal of the American Society for Mass Spectrometry* 29, no. 6 (2018): 1295–1307, https://doi.org/10.1007/s13361-018-1943-9.

34. H. Buck-Wiese, M. Fanuel, M. Liebeke, et al., "Discrimination of Beta-1,4- and Beta-1,3-Linkages in Native Oligosaccharides via Charge Transfer Dissociation Mass Spectrometry," *Journal of the American Society for Mass Spectrometry* 31, no. 6 (2020): 1249–1259, https://doi.org/10.1021/jasms.0c00087.

35. D. Ropartz, P. Li, G. P. Jackson, and H. Rogniaux, "Negative Polarity Helium Charge Transfer Dissociation Tandem Mass Spectrometry: Radical-Initiated Fragmentation of Complex Polysulfated Anions," *Analytical Chemistry* 89, no. 7 (2017): 3824–3828, https://doi.org/10.1021/acs.analchem.7b00473.

36. D. Ropartz, A. Giuliani, M. Fanuel, C. Hervé, M. Czjzek, and H. Rogniaux, "Online Coupling of High-Resolution Chromatography With Extreme UV Photon Activation Tandem Mass Spectrometry: Application to the Structural Investigation of Complex Glycans by Dissociative Photoionization," *Analytica Chimica Acta* 933 (2016): 1–9, https://doi.org/10.1016/j.aca.2016.05.036.

37. S. Ickert, S. Beck, M. W. Linscheid, and J. Riedel, "VUV Photodissociation Induced by a Deuterium Lamp in an Ion Trap," *Journal of the American Society for Mass Spectrometry* 30, no. 10 (2019): 2114–2122, https://doi.org/10.1021/jasms.8b06228.

Supporting Information

Additional supporting information can be found online in the Supporting Information section.